Accepted Manuscript

Behaviour of corroded Reinforced Concrete beams repaired with NSM CFRP rods, Experimental and Finite Element Study

Belal Almassri, Firas AL. Mahmoud, Raoul Francois

PII: S1359-8368(15)00039-6

DOI: 10.1016/j.compositesb.2015.01.022

Reference: JCOMB 3371

To appear in: *Composites Part B*

Received Date: 17 December 2014

Accepted Date: 13 January 2015

Please cite this article as: Almassri B, Mahmoud FA, Francois R, Behaviour of corroded Reinforced Concrete beams repaired with NSM CFRP rods, Experimental and Finite Element Study, *Composites Part B* (2015), doi: 10.1016/j.compositesb.2015.01.022.

Behaviour of corroded Reinforced Concrete beams repaired with NSM CFRP rods, Experimental and Finite Element Study

Belal ALMASSRI (1), Firas AL MAHMOUD (2), Raoul FRANCOIS (1)

(1) *Université de Toulouse; UPS, INSA, LMDC (Laboratoire Matériaux et Durabilité des Constructions), Toulouse, France*

(2) *Institut Jean Lamour, UMR 7198, CNRS, Université de Lorraine, Nancy, France*

Keywords: corrosion, repair, RC beams, NSM rods, failure mode, FEM, FEMIX, ABAQUS

Corresponding author: Firas Al Mahmoud

firas.al-mahmoud@univ-lorraine.fr

ABSTRACT

The near surface mounted reinforcement (NSM) technique is one of the promising techniques used nowadays to strengthen reinforced concrete RC structures. In the NSM technique, the Carbon Fibre Reinforced Polymer (CFRP) rods are placed inside pre-cut grooves and are bonded to the concrete with epoxy adhesive. This paper investigates corroded RC beams repaired with NSM CFRP rods and studies the failure mode of the repaired beam according to experimental and numerical modelling results. Experimental results and numerical modelling results of a 2D finite element (FE) model using the FEMIX computer code were obtained on five, 3-metre-long beams: three corroded RC beams that had been exposed to natural corrosion for 25 years and two control beams with no corrosion. Two beams, one corroded and one control (A1CL3-R and A1T-R) were each repaired in bending with one 6-mm-diameter NSM CFRP rod and were then tested in three-point bending up to failure. The corrosion of the tensile steel bars and steel stirrups was studied. Ultimate capacity, yielding capacity and failure modes are also discussed. The experimental results showed that the NSM technique increased the overall capacity (ultimate load capacity and yielding capacity) of control and corroded beams despite a non-classical mode of failure with separation of the concrete cover occurring in the corroded beam due to damage induced by corrosion. The FE numerical modelling results from FEMIX were compatible with the experimental ones except for the repaired corroded beam A1CL3-R, for which a three-dimensional model using the commercial software ABAQUS was required. Finally some comparisons were made between the experimental and FE numerical modelling results obtained using ABAQUS in order to

study the specific mode of failure of the corroded beam, which occurred by the separation of concrete cover.

1. Introduction

Corrosion of reinforcing steel is still a very important area of study for reinforced concrete structures as the cost induced by repairs to corroded RC structures world-wide exceeds $1.8 trillion per year (1). Much research has been conducted to assess the damage to corroded RC structures. (2–4) presented such damage, starting from the reduction of cross sectional area of the steel and reduction of its ductility and ending with cracking and bonding problems in the RC elements, which lead to the early failure of structures.

The near surface mounted reinforcement (NSM) technique is one of the most promising techniques used nowadays for strengthening deteriorated structures. In the NSM technique, the Carbon Fibre Reinforced Polymer (CFRP) rods are placed inside pre-cut grooves and are bonded to the concrete with epoxy adhesive. (5–8) have shown that the NSM strengthened members can be expected to be much more ductile than externally-bonded-laminate (EBR) strengthened members and fail at much higher strain levels. De Lorenzis and Teng (9) showed also some of the advantages of the NSM technique over the EBR strengthening technique: (1) the NSM installation process is less time consuming, (2) the NSM reinforcements are protected from natural and accidental damage and (3) the NSM technique has better bonding as the FRP rod is fully embedded in this case. In addition, Bilotta et al. (10) showed that the tensile strength of FRP material used in the NSM technique was well exploited and debonding was delayed compared to the EBR technique.

Kreit et al. (11) and Al-Mahmoud et al. (12) indicated that the use of NSM reinforcement could significantly improve the flexural performance of the RC beams by increasing their ultimate load-bearing capacity, and Almassri et al. (13) showed that the NSM technique also restored sufficient ductility (2.8 times that of the non-repaired corroded beams) despite the ductility loss of steel bars induced by corrosion.

The experimental data presented by Al-Mahmoud et al. (12) was used later by Hawileh (14), who presented an FE model that could predict the ultimate capacity of RC beams subjected to 4-point loading using the commercial FEM-based computer software ANSYS. It was found that the diameter of the FRP reinforcement rod had a crucial effect on the stiffness and the ultimate capacity of the RC beams strengthened with NSM, the use of 16-mm-diameter FRP rod increasing the ultimate capacity by 83.6% compared to that of a beam strengthened with a 6-mm-diameter rod.

The computer code FEMIX has been used by several researchers to simulate RC beams strengthened with NSM strips. Sena Cruz et al. (15) showed that the epoxy adhesive had a negligible effect on the global behaviour and the crack pattern and load-deflection curves obtained numerically in this study matched the experimental results.

The FEM-based computer software ABAQUS has been used several times to simulate RC beams, as by Lundqvist et al. (16), who studied the anchorage length of CFRP rod needed to prevent premature failure, while Radfar et al. (17) used ABAQUS to study the peeling-off failure mode in beams strengthened with externally bonded FRP laminates. Another study Kang et al. (18) used ABAQUS in order to study the percentage increase of the load bearing capacity when using different groove depths of NSM FRP laminates as a strengthening technique. Few studies have used FE models to investigate the mechanical behaviour of corroded RC beams repaired with the NSM CFRP rod technique.

The present paper studies the performance of five RC beams: one corroded and one control (non-corroded) repaired in bending with the NSM CFRP rod technique, and three non-repaired corroded and control beams. All beams were tested statically in three-point loading up to failure. The failure modes, and the ultimate and the yield moment capacities for all beams were studied. An FE model for all RC beams was created using the computer code FEMIX, and the moment-deflection curves and the modes of failure were compared to the experimental results. A high degree of compatibility was found between experimental and FEM results even though the 2-D model in FEMIX was not able to capture all aspects of corroded repaired beam A1CL3-R (e.g. the sufficient deflection at failure). It was necessary to implant a 3-D model in order to investigate the specific mode of failure of RC beam A1CL3-R using the commercial software ABAQUS.

2. Experimental programme

An experimental programme was started at LMDC (Laboratory of Materials and Durability of Constructions) in 1984 with the aim of understanding the effects of steel corrosion on the structural behaviour of RC elements. Many experimental studies have been conducted on those beams to evaluate the development of corrosion cracking, to measure chloride content, and to analyse the change of mechanical behaviour (19,20). The natural aggressive environment system is presented in (11).

The five beams studied in this paper were of the same type (the same size and shape of reinforcement but different values of service loading). One corroded beam (A1CL3-R) and one control beam (A1T-R) were repaired with one 6-mm-diameter CFRP rod and tested in bending by (13). Long-term corroded beams A2CL1 and A2CL3, and control beam A2T tested by (21,22) but not repaired were also used here for comparison.

Two loading values were applied: Mser1 = 13.5 kN.m for beams referred to as A1 (A1CL3-R and A1T-R) and Mser2 = 21.2 kN.m for beams referred to as A2 (A2CL1, A2CL3 and A2T). The layout of the reinforcement is shown in Figure 1. For these beams, Mser represented the maximum loading value versus durability in an aggressive environment (serviceability limit-state requirements in an aggressive environment).

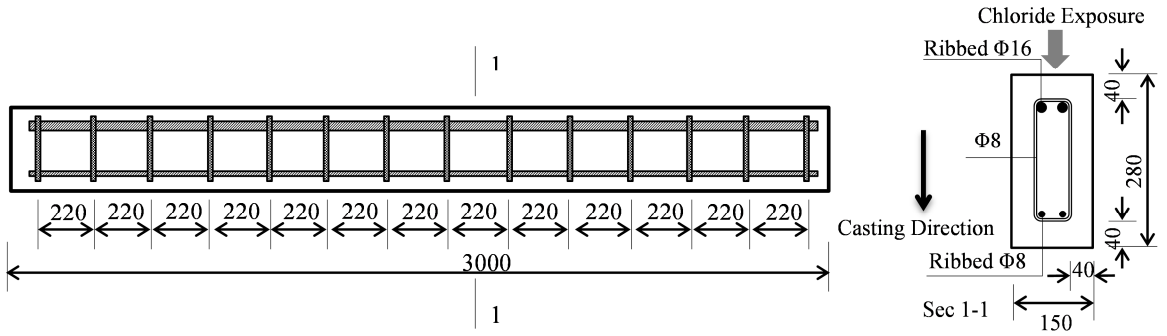

Figure 1 Reinforcement layout of type A beams. Dimensions are in mm

2.1 Material properties

2.1.1 Concrete properties

The average compression strength and the elastic modulus obtained on cylindrical specimens (11 cm diameter ×22 cm height) were 45 MPa and 32 GPa respectively at 28 days. The tensile strength, measured using the splitting test, was 4.7 MPa. Water Porosity was 15.2%. To measure the present-day characteristics of the concrete, 70 × 140 mm cylindrical cores were

drilled out of each beam and tested in both compression and tension. Table 1 shows the results of these core tests.

Table 1 Mechanical characteristics of the concrete at 27 years (average values of 3 tests)

Mechanical characteristics	A1CL3-R	A1T-R	A2T	A2CL3	A2CL1
Compression strength (MPa)	62.2	58.9	58.5	61.5	58.8
Tensile strength (MPa)	6.85	6	6	6.2	6
Elastic modulus (MPa)	34 000	30 000	32 000	32 000	32 000

2.1.2 Characterization of steel Bars, CFRP Bars and filling material

The ordinary ribbed reinforcing steel bars used were composed of natural S500 half-hard steels. The characteristics of the steel bars were measured after extracting the corroded bars from the corroded beam A1CL3-R and non-corroded bars from the control beam A1T-R. The specimens consisted of two corroded and two control steel bars of 400 mm length (the corroded steel bar specimens were extracted from the beam near the maximum corrosion pit found, as shown in figure 5) and their properties are presented in Table 2. The behaviour of corroded steel bars was the same as found by (23): the true yielding stress was the same for control and corroded specimens; the ultimate stress was higher for corroded than for control specimens as the brittle failure induced by corrosion strongly reduced the necking effect, which is not taken into account to calculate actual ultimate stress. The corrosion led to a brittle failure of bars in tension which was characterized by a strong reduction in ultimate elongation.

Table 3 shows the mechanical properties of the CFRP rods found in François' paper and the mechanical properties given by the manufacturer and by laboratory tests (24). In order to increase the bond between the CFRP rods and the filling material, the CFRP rods were coated with 0.2/0.3 mm of surface sanding material, which was sprinkled onto an epoxy resin applied to the surface of the rods. Table 4 shows the characteristics of the filling material (epoxy resin) after 7 days according to the manufacturer.

Table 2 Average values of steel bar properties

Specimen Type	Young's modulus (GPa)	Yield Strength (MPa)	Ultimate Strength (MPa)	Ultimate strain
Corroded specimen	200	550	604	4%
Non-corroded specimen	200	550	645	8%

Table 3 CFRP rod characteristics.

Type of test	Ultimate strength (MPa)	Modulus of Elasticity (MPa)
Manufacturer's test	2300	150000
Laboratory test	1875	145900

Table 4 Filling material properties according to the manufacturer

Material	Compressive Strength (MPa)	Tensile Strength (MPa)	Elastic Modulus (MPa)
Epoxy	83	29.5	4900

Figure 2 shows the experimental tensile stress-strain curves for corroded steel bars, non-corroded steel bars and CFRP rods.

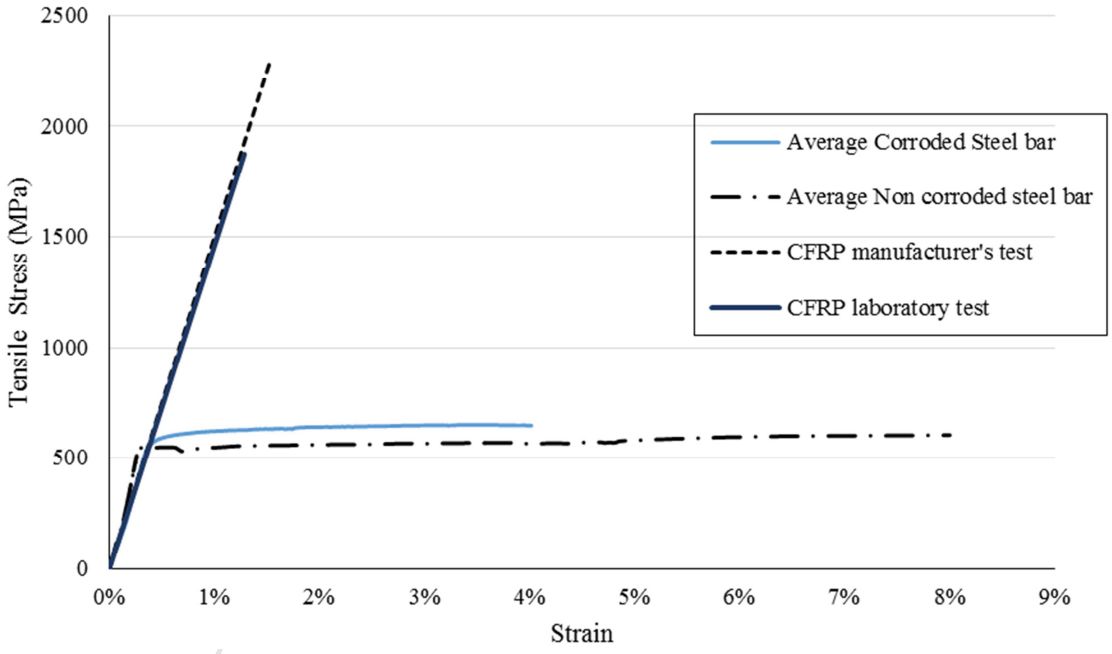

Figure 2 Tensile stress-strain curves for steel and CFRP rods (Corroded and control steel bar curves are average results of 2 tested specimens in each case)

2.2 NSM repair technique

The NSM CFRP rod was installed in the corroded beam A1CL3-R and in the control beam A1T-R by making two cuts in the concrete cover in the longitudinal direction at the tension side. A special concrete saw with a diamond blade was used. The groove was 15 mm deep (only 20 mm of concrete cover for beams) and 15 mm wide (around 2.5 times the rod diameter) (25). Figure 3 presents the main steps of this repair process while figure 3 shows the final shape of the repaired beams after their surfaces had been levelled.

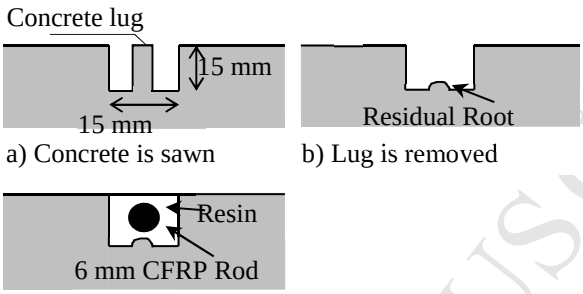

a) Concrete is sawn b) Lug is removed

c) Rod is embedded in the groove

Figure 3 Installation of CFRP rod in concrete surface

The two beams were tested 1 week after the installation of the CFRP rod in order to ensure the maximum degree of adhesion between the concrete surface and the epoxy resin material. Figure 4 shows the concrete surfaces of the RC beams after the installation the CFRP rods.

a. A1T Control Beam b. A1CL3 Corroded Beam

Figure 4 Concrete surfaces after installation of the CFRP rod.

3 Experimental results

3.1 Corrosion damage of the steel bars in corroded beam A1CL3-R

The values of the diameter losses were measured for both the Back Side (BS) and Front Side (FS) tensile steel bars which were extracted from the corroded beam A1CL3-R just after the bending test. The maximum diameter loss was found to be 38% at 120 cm from the left edge of the beam. The corrosion was found both at the top of the bars close to the surface cover, reflecting the classical result for natural corrosion (26), and at the bottom of the bars, reflecting the effect of casting direction and bar location at the top of the beam, known as "Top-bar effect" (27,28).

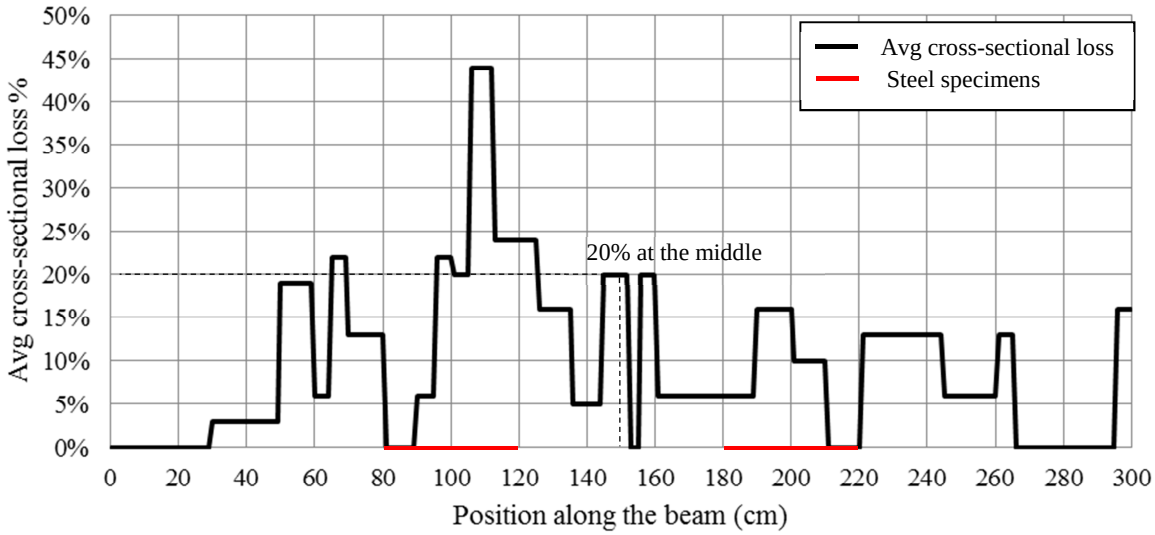

Figure 5 Average cross-section loss percentages in corroded beam A1CL3-R.

Figure 5 shows the average loss of cross-section along the beam calculated from both tensile bars. Despite the presence of a large local loss of steel cross-section at 110 cm from the beam end and 40 cm from the point load, the experimental results did not show any failure of steel re-bars during the bending test. It is therefore assumed that the yielding of steel during the loading occurred at mid-span, where the average loss of cross-section was 20%.

The steel stirrups were also measured for corrosion and it was found that stirrup corrosion was mostly located on the horizontal part of stirrups at the top of the beam according to the casting direction. This was related to the corrosion of tensile steel bars, while compressive steel bars showed corrosion pits only. It was assumed that stirrup corrosion did not influence the residual bending behaviour of corroded beams, so it was not taken into account in the modelling.

3.2 Response in bending for both corroded and non-corroded repaired beams

The two repaired beams A1CL3-R and A1T-R were tested with 3-point loading up to failure. More details of the experimental set-up can be found elsewhere (13). Figure 6 shows the bending moment versus the deflection for the two beams. The ultimate moment values were 52 kN.m and 66 kN.m respectively. Yielding and ultimate bending moment were reduced to similar extents: by 12 kN.m and 13.5 kN.m respectively. The ultimate elongation was reduced by 33%, which is quite considerable even though non-repaired corroded beams have exhibited more brittle behaviour (more than 50% of reduction) in previous studies (29).

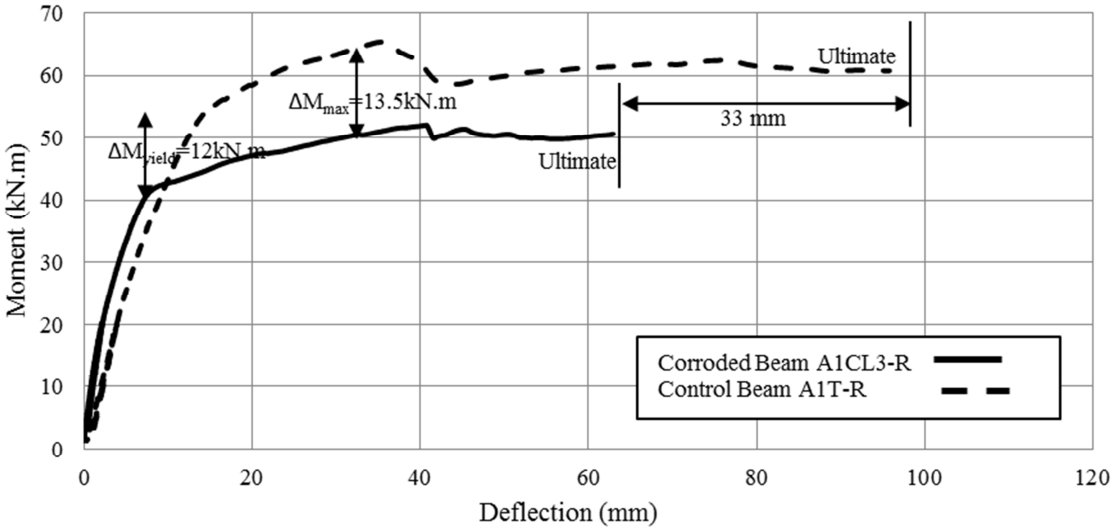

Figure 6 Moment-deflection curves for beams A1CL3-R and A1T-R tested experimentally

3.3 Failure modes

The failure mode of non-repaired type A beams is usually due to steel bar yielding followed by concrete crushing (21). After strengthening with NSM FRP rod, the RC beams may fail by concrete crushing, pull-out of the FRP rods or peeling-off as shown by (12). The failure of the repaired control beam A1T-R occurred by the crushing of compressed concrete while the failure mode observed for A1CL3-R was different from both the conventional and non-conventional failure modes found on non-corroded repaired beams. The failure of the repaired corroded beam A1CL3-R was due to the separation of the concrete cover as shown in Figure 7. It is also important to note that failure of the RC beams tested here was not due to brittle failure of the tensile corroded steel bars as usually found by previous studies on corroded RC beams (19–21,29).

a) A1CL3-R Corroded a) A1T-R Control Beam

Figure 7 Experimental failure modes

4. Numerical modelling

FEMIX 4.0 is a computer code that has the ability to analyse structures by using the Finite Element Method (FEM). FEMIX code is integrated with GiD interface software which provides pre- and post-processing for numerical simulations analysis. FEMIX is based on the displacement method; it has a large number of types of finite elements inside, such as 3D frames and trusses, plane stress elements, flat or curved elements for shells, and 3D solid elements. Linear elements may have two or three nodes while plane stress elements may have 4, 8 or 9 nodes and 8 or 20 hexahedral nodes. Embedded line elements can be included in the analysis with the availability of static or dynamic tests using both linear and non-linear material configurations. Advanced numerical techniques are available, such as the Newton-Raphson method combined with arc-length techniques and path dependent or independent algorithms.

4.1 Concrete properties

An elasto-plastic multi-fixed smeared crack model was created on GiD FEMIX in order to define the concrete material (15). When the crack occurs in a sampling point, the total incremental strain becomes a sum of reversible elastic strain and irreversible plastic (crack) strain. The crack strain is controlled by the fracture parameters of the material, The Rankine criterion was used to define the concrete in tension and the Owen and Figueiras (30) yield surface was used to define the concrete in compression. The crack evolution in fracture mode was simulated using a tri-linear tension softening or stiffening diagram as shown in figure 8.

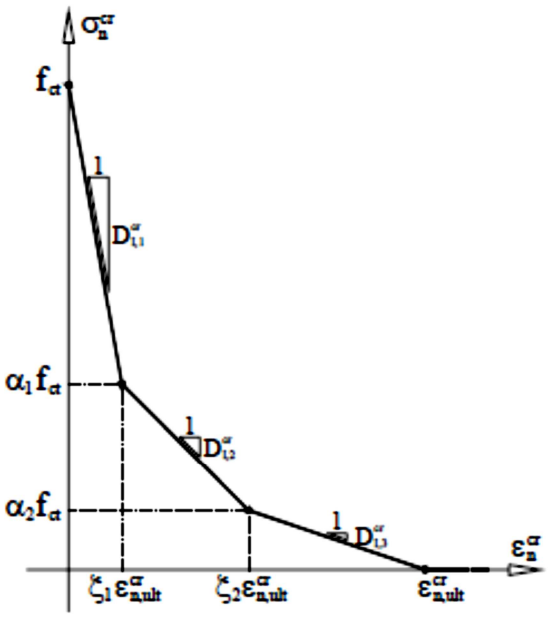

Figure 8 Tension softening diagram for concrete

Table 5 presents the concrete properties used in the numerical simulations. From the mean value of the experimentally obtained compressive strengths, all the other parameters were estimated. The post-cracking behaviour of the reinforced concrete was simulated using a tri-linear tensile-softening diagram.

Table 5 concrete properties used in FEMIX simulation analysis

Poisson's ratio	$\nu_c = 0.20$
Initial Young's modulus	$E_c = 30\,000$ N/mm^2
Compressive strength	$f_c = 60$ N/mm^2
Tri-linear tensile-softening diagram	$f_{ct} = 4.5$ N/mm^2 , $G_f' = 0.09$ N/mm $\xi_1 = 0.005$, $\alpha_1 = 0.5$, $\xi_2 = 0.3$, $\alpha_2 = 0.2$
Parameter defining the mode I fracture energy available to the new crack	$P_2 = 1$
Threshold angle	$\alpha_{th} = 30^o$

4.2 CFRP rods

The CFRP rod was modelled with an elastic stress-strain curve up to brittle failure in tension according to the manufacturer's criteria (tensile stress-strain curve is shown in Figure 2).

4.3 Steel reinforcement properties

The non-linear behaviour of the steel reinforcement bars was considered to be elastic-plastic. A Poisson's ratio of 0.3 was used, and the elastic modulus and yield strength values of the steel reinforcement bars and stirrups were as shown in Table 2. The post yielding hardening

behaviour of the steel bars was modelled as shown in figure 10 (a) and (b). From the experimental tensile stress-strain results for steel bars (shown in figure 2), it was found that the ultimate strain value for the corroded steel bars was equal to half the ultimate strain value for non-corroded steel bars - the same result as obtained by Dang and François (31). The average ductility factor (εu-corroded/ εu) was reduced to 0.5 for RC beams having cross-sectional loss of over 15% in the tensile steel bars, as shown in figure 9.

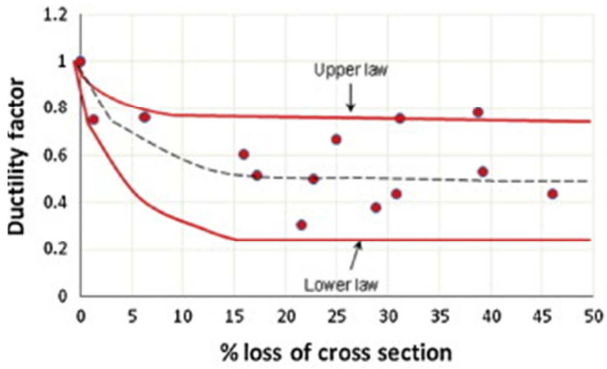

Figure 9 Ductility factor ($\varepsilon_{ucorroded}/\varepsilon_u$) for steel bars versus corrosion, from Dang & Francois (31)

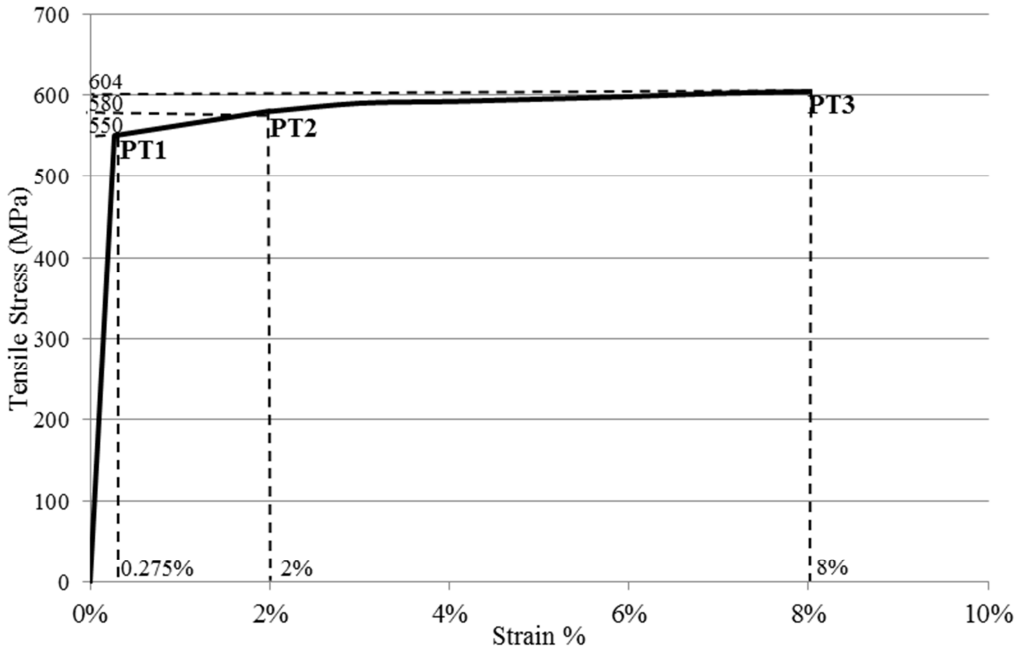

Figure 10 (a) uniaxial constitutive model for non-corroded rebar

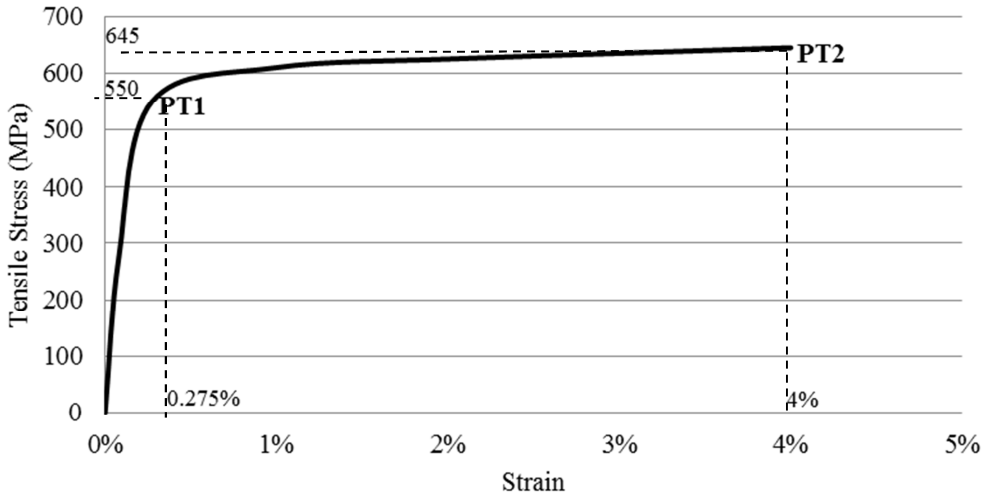

Figure 10 (b) uniaxial constitutive model of corroded rebar

4.4 Modelling of RC beams

The objective of this part is to create a reliable numerical model that can simulate and predict the global behaviour of five RC beams and analyse the NSM strengthening effect in bending. Two of the beams were control beams: A1T-R, A2T and the other three were corroded: A1CL3-R, A2CL3 and A2CL1 (A1T-R and A1CL3-R were RC beams strengthened with NSM CFRP rod in bending). To simulate the concrete in the beams, 8-node plane stress elements with 3×3 Gauss-Legendre integration were used. The steel bars and stirrup reinforcements, and the CFRP rods, were simulated using 3-node quadratic embedded cable elements with two Gauss-Legendre integration points. For this point, the steel bars and stirrups, as well as the CFRP rods, were assumed to be fully bonded with the concrete. Figures 11 and 12 show the geometry, elements mesh, loading and support configuration.

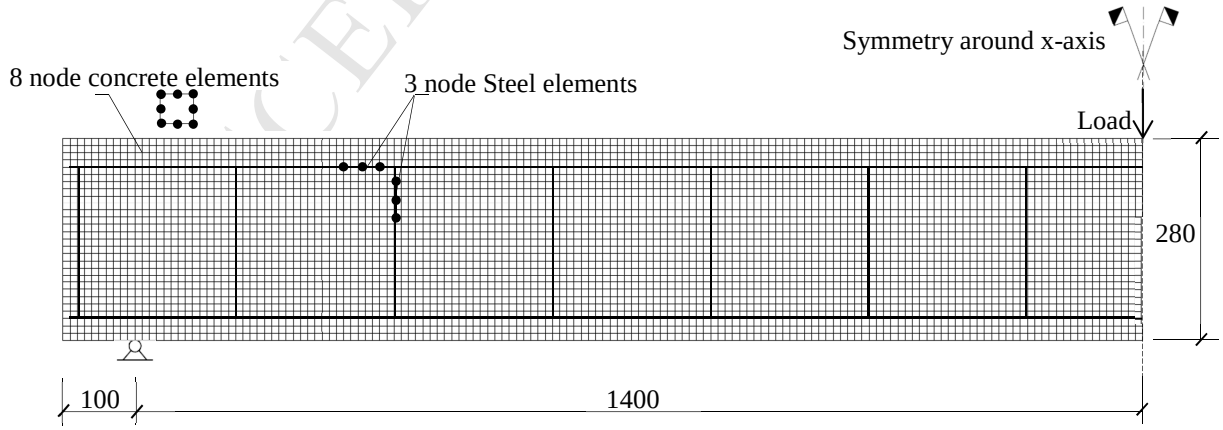

Figure 11 Geometry in (mm), mesh, loading and support conditions for non-strengthened beams with NSM CFRP

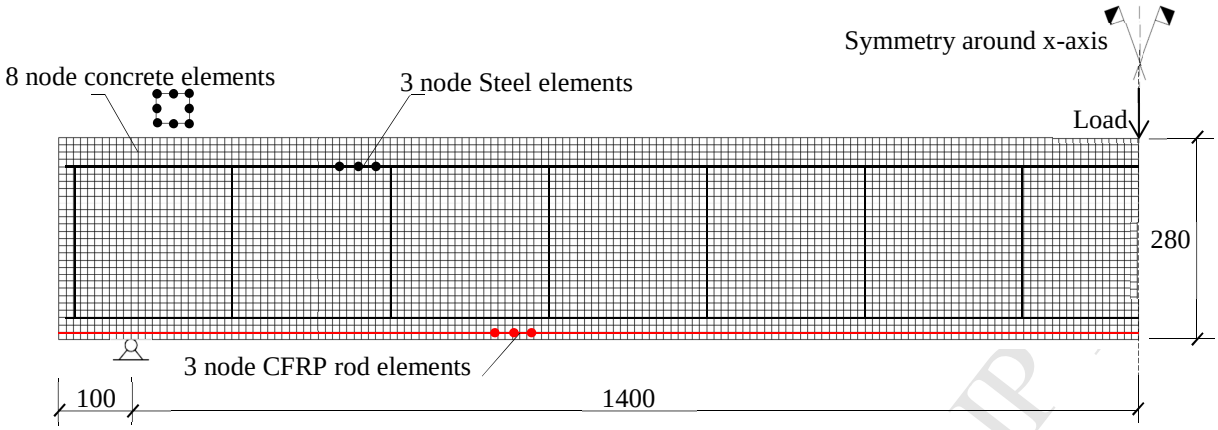

Figure 12 Geometry, mesh, loading and support conditions for strengthened beams with NSM CFRP

4.4.1 Corroded RC beams

The main goals of the numerical modelling were to capture the changes in yielding capacity, ultimate capacity and ultimate deflection values of the RC beams due to the corrosion of the reinforcing steel bars. As a result, the residual re-bar cross-section at the failure location was used here for all corroded RC beams that failed due to the failure of corroded tensile steel bars. The residual re-bar cross section was assumed to be constant all along the reinforced concrete beams. For RC beams that did not fail by brittle failure of corroded tensile steel bars, the residual steel cross-section at mid span was used as the constant cross section all along the beam. Moreover a perfect bond was assumed between the re-bars and the concrete, even in cases of corrosion of the reinforcement. This assumption did not allow the change in bending stiffness due to corrosion to be modelled. Both the decrease in the steel-concrete bond and the variability in the change of steel-cross section induced by corrosion along the beams have an influence of the load-deflection response of corroded beams.

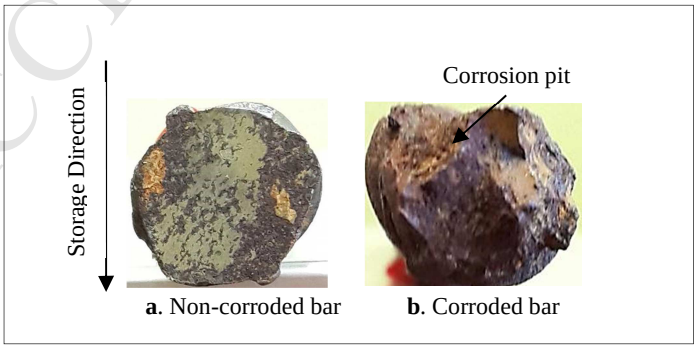

Figure 13 corrosion pits in tensile steel bars of corroded RC beam

A reduction of 20 % of the steel cross-section was considered for the repaired RC beam A1CL3-R (13), while the percentage values for beams A2CL3 and A2CL1 were considered to

be 21.5 % and 30 % respectively (21). The reduction of the tensile steel bar diameters was not uniform in shape due to the existence of corrosion pits (shown in figure 13). The corrosion in steel stirrups was not considered in this model as it would have no effect on the flexural behaviour of the RC beams.

4.4.2 Results for all beams

Figure 14 shows the load-deflection curves for all beams tested experimentally, together with the numerical modelling results from 2-D FE modelling using the FEMIX computer code.

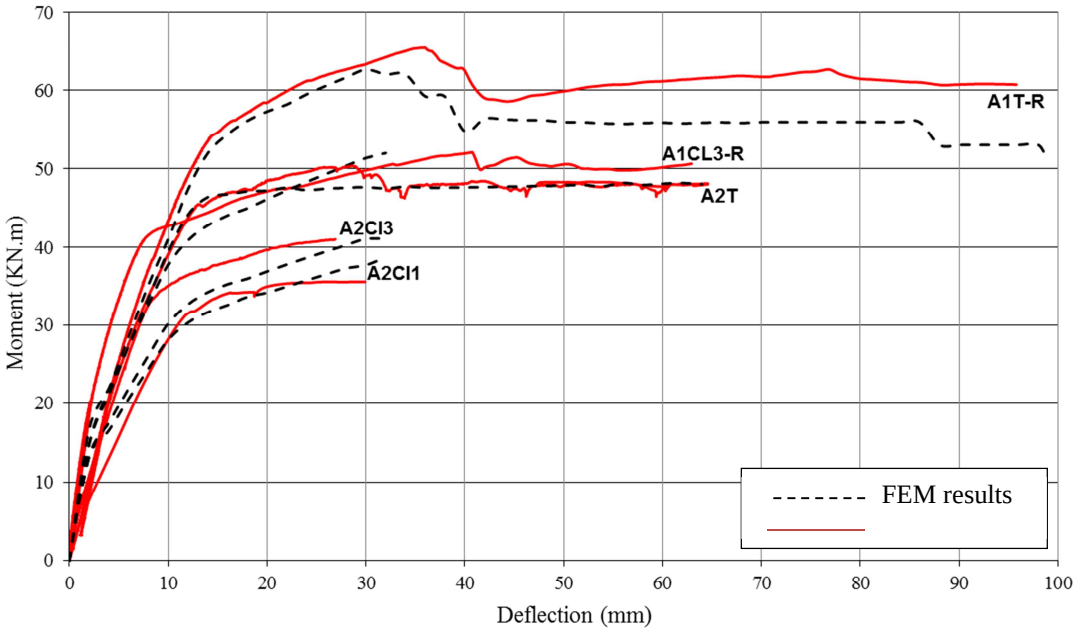

Figure 14 Load Deflection curves for all beams using FEMIX

The start of yielding of the steel reinforcements and the ultimate load carrying capacity were well predicted by the numerical models for all beams. The reduction in ultimate deflection of corroded beams was also well predicted by the model as the change in steel ultimate elongation induced by corrosion which was implemented in the modelling

The post-yielding behaviour of corroded beams appeared to be stiffer than that of control beams due to a harder post-yielding behaviour of corroded steel bars than of controls (as shown in figure 10)

The only exception occurred in beam A1CL3-R, where the predicted ultimate deflection appeared to be half the experimental value. Moreover, it was the only beam with corroded steel that did not collapse by brittle failure of the tensile steel bars, so modelling would be expected to predict a higher deflection. Thus it seems that the 2D model approach implemented could not model the behaviour of corroded RC beams repaired with NSM rods.

Moreover, corroded repaired beam showed a non-classical mode of failure with separation of the concrete cover. Thus, the need for a 3D model to investigate this special mode of failure was highly evident for this point. Figure 15 presents a sample of the classical crack failure pattern that occurred for all beams, with large flexural cracks at the middle along with crushing of the concrete.

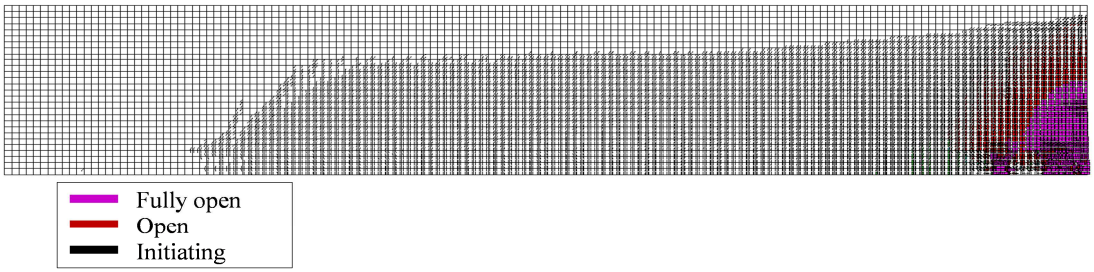

Figure 15 2D crack failure pattern using FEMIX

4.5 Three-dimensional model for RC beam A1CL3-R

The objective of this part was to create a 3-D model that could accurately predict the moment deflection curve, the global behaviour and the mode of failure for the corroded RC beam repaired with NSM CFRP rod in bending (A1CL3-R), using the commercial software ABAQUS. In this 3-D model, the concrete material and the filling material (epoxy resin) were simulated using an ABAQUS 3-D deformable solid structural element while a 3-D deformable wire was used to simulate the steel bars, the steel stirrups and the CFRP NSM rod reinforcement using a truss element. The steel loading plate and the steel supports were simulated using a 3-D deformable solid element and they were given higher yield values than the steel bars and stirrups in order to prevent early yielding.

4.5.1 Concrete properties

The mechanical behaviour of concrete is difficult to simulate because of its complexity in traction and compression and its brittle cracking. Nowadays, many models can simulate concrete material using different approaches, such as the concrete smeared cracking approach (32,33), the concrete damaged plasticity approach (16,34) and the discrete cracking approach (35).

In this part, the mechanical properties of concrete found experimentally and listed in Table 1 were used in ABAQUS to define the characteristics of concrete material with a Poisson's ratio of 0.2. The plastic behaviour of concrete in compression was defined using the Drucker-Prager yield function, which is controlled by the Drucker-Prager hardening variables in

tension and compression. The Drucker-Prager criterion is a smooth approximation of the Mohr-Coulomb yield surface and it is controlled with two parameters: cohesion, C, and internal angle of friction, Ø. It can be expressed using equation (1):

$$f(I_1, J_2) = \alpha I_1 + \sqrt{J_2} - k = 0 \qquad \text{Eq.(1)}$$

Where α, k are Drucker-Prager material constants, I_1 is the first invariant of the effective stress tensor and J_2 is the second invariant of the stress deviator tensor. In cases where the Drucker-Prager passed the inner cone of the tension meridian of the Mohr-Coulomb hexagon, the Drucker-Prager constants were expressed using equations (2):

$$\alpha = \frac{2\sin\emptyset}{\sqrt{3}(3+\sin\emptyset)}, k = \frac{6c\cos\emptyset}{\sqrt{3}(3+\sin\emptyset)} \qquad \text{Eq.(2)}$$

The two parameters, cohesion C and internal angle of friction Ø, were assumed to be C =2.8 MPa and Ø = 32˚ as recommended by (36). The results of the experimental concrete specimens tested in compression were used in ABAQUS to fill in the Drucker-Prager hardening values and the Young's moduli of concrete beams shown in Table1 were used.

The same modulus of elasticity and Poisson's ratio were used here with the same tensile strength values obtained by the uniaxial traction tests as shown in Table 1. Figures 16 and 17 show the Drucker-Prager failure criterion and the tension softening of the concrete respectively.

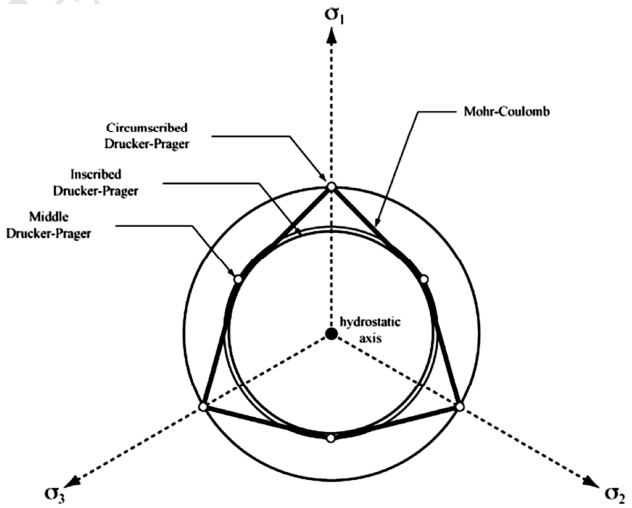

Figure 16 Drucker-Prager failure criterion in stress space (32)

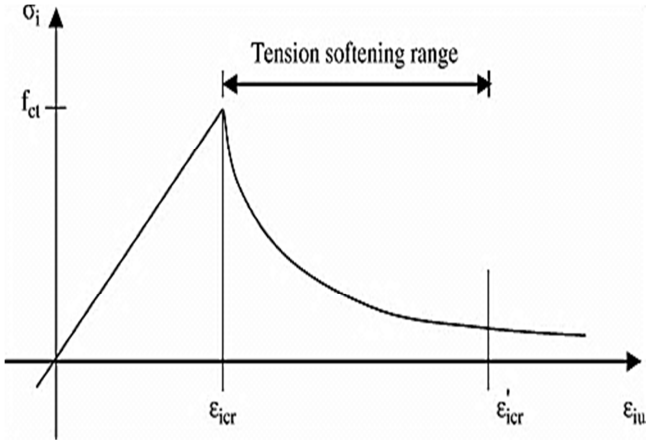

Figure 17 Tension softening of concrete

4.5.2 Steel properties

The steel reinforcement bars and stirrups were considered to have linear elastic-plastic behaviour. The post yielding hardening behaviour used in FEMIX and shown in figure 10 (b) was used again in ABAQUS for the corroded steel bars. The reduction in ultimate elongation induced by corrosion was also the same in ABAQUS as it was in FEMIX.

4.5.3 CFRP rods and filling material

The mechanical properties of the epoxy resin material and the CFRP rods used in this model were exactly the same as those found in the experimental tests and given in Tables 3 and 4. The filling material was modelled as a 3-D solid element while the cracking model of concrete was also used here in order to simulate the plastic behaviour of epoxy material. The CFRP rod was modelled by an elastic stress-strain curve up to brittle failure in tension and zero strength in compression, a method already used in a previous study (14).

4.5.4 Simulation of corrosion cracks

The corrosion cracks shown in figure 18 were considered to be the main reason why the separation of concrete cover was the mode of failure for the repaired corroded beam. This plane of cracks was simulated using a crack tool in the interaction section in ABAQUS as shown in figure 19. The cross-sectional area of the tensile steel bars of corroded beam A1CL3-R was reduced due to the corrosion and they were given an average corrosion value (20% for tensile steel bars) at the middle of the beam.

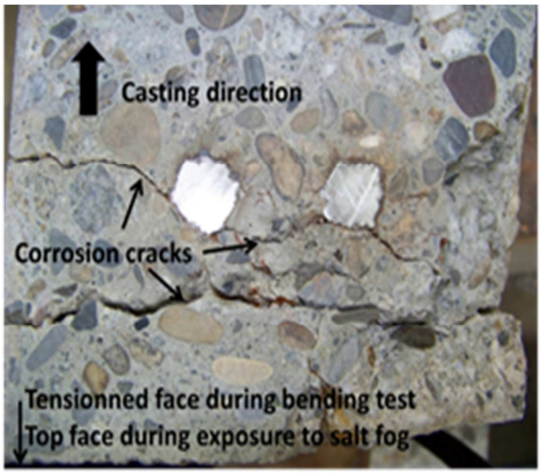

Figure 18 Corrosion-induced cracks appear in the concrete cover from the steel part closest to the tensioned surface exposed to chloride for type “A" beams (Almassri et al.(13))

In order to define the crack lines along the concrete cover of the corroded RC beam A1CL3-R2 FEM, several steps were employed (ABAQUS/CAE User’s Manual):

1. Several partitions were drawn just where the cracks appeared in the concrete cover as shown in figure 19.
2. The crack line was defined using a crack tool from the interaction module in ABAQUS by selecting element edges of the partitioned parts that formed continuous lines.
3. The crack extension direction was defined normal to the crack plane (across the beam width) in order to simulate the corrosion cracks described in figure 18.
4. Finally, a seam crack was defined along the crack plane edges. This crack was defined by ABAQUS as an edge or a face in the model, which was originally closed but could open during the analysis.

The existing vertical flexural cracks were also added in order to simulate the real state of pre-loading of the corroded beam.

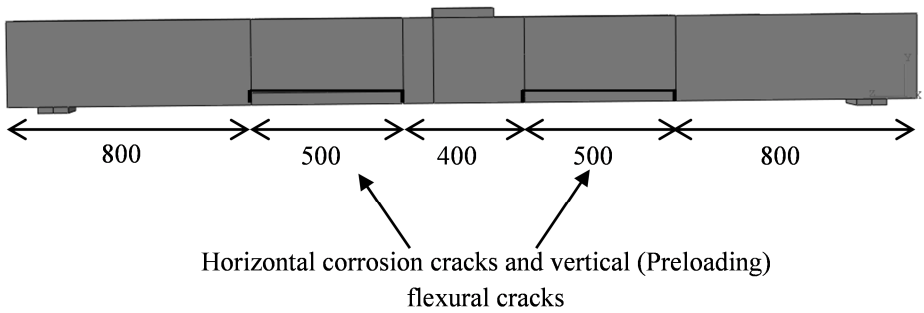

Figure 19 Cracks created at concrete cover plane of corroded beam in (mm)

4.6 FEM numerical model

4.6.1 General description

A 3-D finite element model was created with the commercial FEM software ABAQUS, which uses a non-linear static procedure with a classical Full-Newton solving method. In this study, the full beam was modelled using suitable boundary conditions as shown in figure 20, all the material discussed previously being inserted.

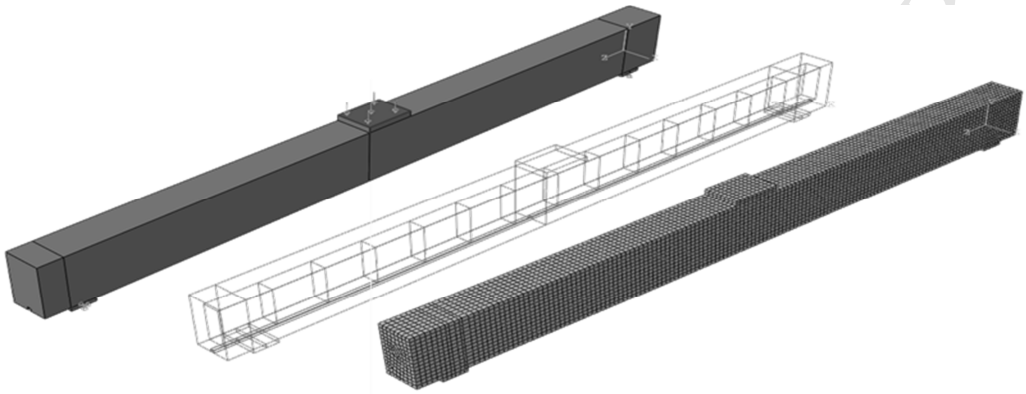

Figure 20 Boundary conditions, steel skeleton and meshing of beam model

As the main objective here is to discuss the failure mode in which there is separation of the concrete cover, a full bond was assumed between FRP and concrete and also between steel reinforcement rebars and concrete material as assumed by Radfar et al. (17) to model a non-conventional failure mode (peeling-off).

4.6.2 Meshing and step size increments

The meshing edge size of 10 mm was used for concrete elements; In order to ensure the maximum degree of accuracy in ABAQUS, a large value was entered as the maximum number of increments (100,000 increments) while a small value (1E-08) was entered for the minimum increment size.

4.7 FEM results of 3D model

4.7.1 Ultimate load capacity and failure mode of RC beam A1CL3-R

Two FEM models were created in ABAQUS. The first one dealt with the repaired corroded RC beam without considering any corrosion cracks (FEM A1CL3-R1) while the other (FEM A1CL3-R2) took the corrosion cracks of the corroded RC beam into account. The moment-deflection curves for both models were drawn at the mid-span point for comparison with the experimental results as shown in figure 21. From simulation results of the RC beam A1CL3-R1, it can be concluded that the 3-D model implemented in ABAQUS captures the recovery

in ultimate deflection that is provided by the NSM rod. This was not the case for the 2-D model in FEMIX.

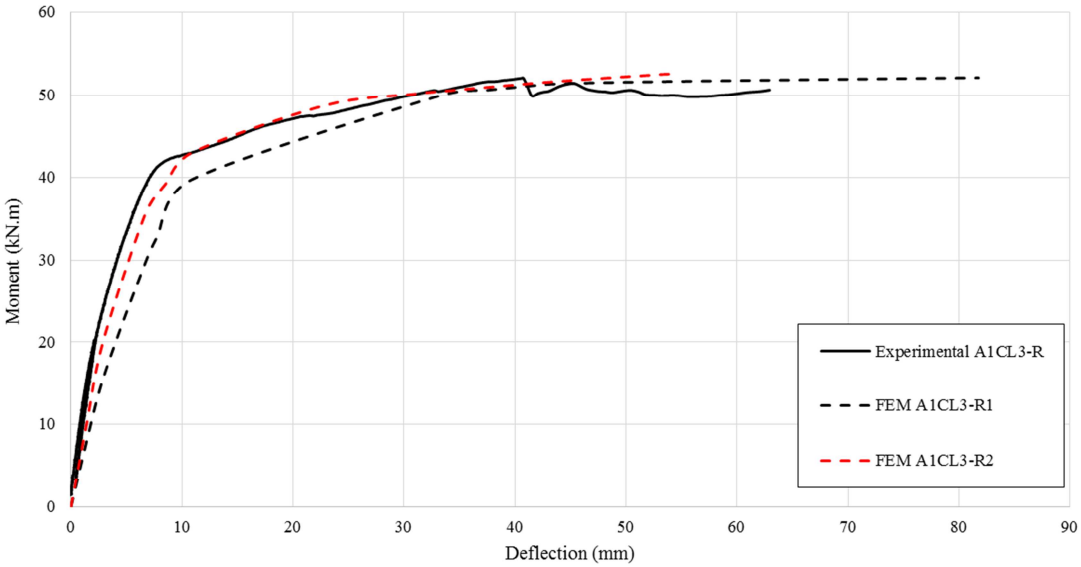

Figure 21 Experimental curves vs. 3D FE Model moment-deflection curves obtained with Abaqus for RC beam A1CL3-R

Nevertheless, the results show that the corroded, non-cracked beam FEM A1CL3-R1 gave higher deflection values than the experimental corroded beam (with 22 mm difference) whereas, when the corrosion crack line was defined in order to simulate premature failure (FEM A1CL3-R2), it gave lower deflection values than the non-cracked beam and results were closer to the experimental ones. Table 6 presents a comparison between experimental and 3-D FEM results for each model in terms of yielding moment, ultimate moment and ultimate deflection.

Table 6 FEM vs. experimental results for A1CL3-R using Abaqus

Beam	Yielding moment (kN.m)	Ultimate moment (kN.m)	Ultimate deflection (mm)
Experimental A1CL3-R	42.3	52	63
FEM A1CL3-R1	39.7	52.2	85
FEM A1CL3-R2	43	52.6	55

The 3D model implanted in ABAQUS captured the failure occurring by the separation of concrete cover near the middle of the beam as shown in figure 22.

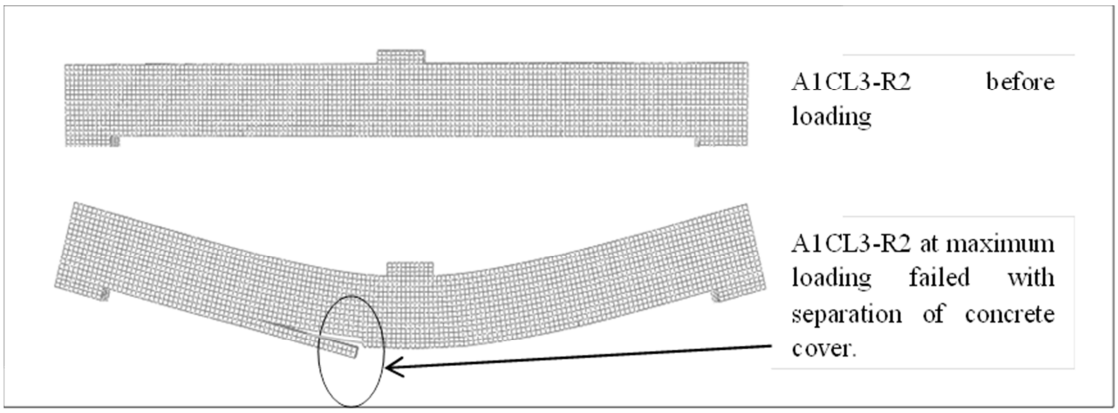

Figure 22 Mode of failure obtained for corroded RC beam A1CL3-R by 3D FE model using Abaqus

5. Conclusions

According to the results found in this work, the following conclusions can be drawn:

1. The NSM technique, which was used to repair corroded RC elements, restored significant ductility by avoiding premature failure of tensile bars at pit locations. However, the presence of cracks induced by corrosion coincident with the tensile reinforcement induced a new premature failure mode.
2. The two-dimensional FEM analysis using FEMIX captured the main aspects observed in the experimental tests, such as yield initiation of the steel bars and load carrying capacity for both repaired and non-repaired corroded and control beams.
3. The two-dimensional FEM analysis using FEMIX captured the reduction of ultimate deflection of non-repaired beams due to the more brittle behaviour of corroded steel in tension but could not capture the ductility recovery induced by the repair with NSM rod.
4. The damage induced by corrosion modifies the flexural response of repaired corroded beams and leads to a new, non-conventional failure mode by separation of concrete cover in the plane defined by the corrosion cracks.
5. Three-dimensional FEM analysis using ABAQUS was able to predict both load-bearing capacity and ultimate deflection reduction due to corrosion if the crack plane induced by corrosion was taken into account in the model.

REFERENCES

1. Schmitt G. Global needs for knowledge dissemination, research, and development in materials deterioration and corrosion control. World Corros Organ N Y. 2009;

2. Al-Sulaimani G, Kaleemullah M, Basunbul I. Rasheeduzzafar,(1990)"Influence of corrosion and cracking on bond behaviour and strength of reinforced concrete members" ACI Structural Journal, 87 (2), 220-231. ASTM G1. 1990;

3. Andrade C, Alonso C, Garcia D, Rodriguez J. Remaining lifetime of reinforced concrete structures: Effect of corrosion on the mechanical properties of the steel. 1991;

4. Cairns J, Plizzari GA, Du Y, Law DW, Franzoni C. Mechanical properties of corrosion-damaged reinforcement. ACI Mater J. 2005;102(4).

5. Hassan T, Rizkalla S. Investigation of bond in concrete structures strengthened with near surface mounted carbon fiber reinforced polymer strips. J Compos Constr. 2003;7(3):248–57.

6. Täljsten B, Carolin A, Nordin H. Concrete structures strengthened with near surface mounted reinforcement of CFRP. Adv Struct Eng. 2003;6(3):201–13.

7. Barros JA, Fortes A. Flexural strengthening of concrete beams with CFRP laminates bonded into slits. Cem Concr Compos. 2005;27(4):471–80.

8. Barros JA, Ferreira DR, Fortes AS, Dias SJ. Assessing the effectiveness of embedding CFRP laminates in the near surface for structural strengthening. Constr Build Mater. 2006;20(7):478–91.

9. De Lorenzis L, Teng J. Near-surface mounted FRP reinforcement: An emerging technique for strengthening structures. Compos Part B Eng. 2007;38(2):119–43.

10. Bilotta A, Ceroni F, Di Ludovico M, Nigro E, Pecce M, Manfredi G. Bond efficiency of EBR and NSM FRP systems for strengthening concrete members. J Compos Constr. 2011;15(5):757–72.

11. Kreit A, Al-Mahmoud F, Castel A, François R. Repairing corroded RC beam with near-surface mounted CFRP rods. Mater Struct. 2011;44(7):1205–17.

12. Al-Mahmoud F, Castel A, François R, Tourneur C. Strengthening of RC members with near-surface mounted CFRP rods. Compos Struct. 2009;91(2):138–47.

13. Almassri B, Kreit A, Al Mahmoud F, François R. Mechanical behaviour of corroded RC beams strengthened by NSM CFRP rods. Compos Part B Eng. 2014;64:97–107.

14. Hawileh RA. Nonlinear finite element modeling of RC beams strengthened with NSM FRP rods. Constr Build Mater. 2012;27(1):461–71.

15. Sena Cruz JM, Barros JA, Gettu R, Azevedo ÁF. Bond behavior of near-surface mounted CFRP laminate strips under monotonic and cyclic loading. J Compos Constr. 2006;10(4):295–303.

16. Lundqvist J, Nordin H, Täljsten B, Olofsson T. Numerical analysis of concrete beams strengthened with CFRP-A study of anchorage lengths. 2005. p. 247–54.

17. Radfar S, Foret G, Saeedi N, Sab K. Simulation of concrete cover separation failure in FRP plated RC beams. Constr Build Mater. 2012;37:791–800.

18. Kang J-Y, Park Y-H, Park J-S, You Y-J, Jung W-T. Analytical evaluation of RC beams strengthened with near surface mounted CFRP laminates. ACI Spec Publ. 2005;230.

19. Castel A, François R, Arliguie G. Mechanical behaviour of corroded reinforced concrete beams—Part 1: experimental study of corroded beams. Mater Struct. 2000;33(9):539–44.

20. Vidal T, Castel A, François R. Corrosion process and structural performance of a 17 year old reinforced concrete beam stored in chloride environment. Cem Concr Res. 2007;37(11):1551–61.

21. Khan I, François R, Castel A. Structural performance of a 26-year-old corroded reinforced concrete beam. Eur J Environ Civ Eng. 2012;16(3-4):440–9.

22. Dang VH, François R. Influence of long-term corrosion in chloride environment on mechanical behaviour of RC beam. Eng Struct. 2013;48:558–68.

23. François R, Khan I, Dang VH. Impact of corrosion on mechanical properties of steel embedded in 27-year-old corroded reinforced concrete beams. Mater Struct. 2013;46(6):899–910.

24. Al-Mahmoud F, Castel A, François R, Tourneur C. Effect of surface pre-conditioning on bond of carbon fibre reinforced polymer rods to concrete. Cem Concr Compos. 2007;29(9):677–89.

25. Al-Mahmoud F, Castel A, François R, Tourneur C, Marchand J, Bissonnette B, et al. Anchorage and tension-stiffening effect between Near-Surface-Mounted Fiber Reinforced polymer rod and concrete. 2006.

26. Yuan Y, Ji Y, Shah SP. Comparison of two accelerated corrosion techniques for concrete structures. ACI Struct J. 2007;104(3).

27. Horne A, Richardson I, Brydson R. Quantitative analysis of the microstructure of interfaces in steel reinforced concrete. Cem Concr Res. 2007;37(12):1613–23.

28. Soylev T, François R. Quality of steel–concrete interface and corrosion of reinforcing steel. Cem Concr Res. 2003;33(9):1407–15.

29. Dang VH, François R. Influence of long-term corrosion in chloride environment on mechanical behaviour of RC beam. Eng Struct. 2013;48:558–68.

30. Owen D, Figueiras J. Anisotropic elasto-plastic finite element analysis of thick and thin plates and shells. Int J Numer Methods Eng. 1983;19(4):541–66.

31. Dang VH, François R. Prediction of ductility factor of corroded reinforced concrete beams exposed to long term aging in chloride environment. Cem Concr Compos. 2014;53:136–47.

32. Chaudhari S, Chakrabarti M. Modeling of concrete for nonlinear analysis Using Finite Element Code ABAQUS. Int J Comput Appl. 2012;44.

33. Si-Larbi A, Agbossou A, Ferrier E, Michel L. Strengthening RC beams with composite fiber cement plate reinforced by prestressed FRP rods: Experimental and numerical analysis. Compos Struct. 2012;94(3):830–8.

34. Abdullah R, Mokhatar SN. Computational analysis of reinforced concrete slabs subjected to impact loads. Int J Integr Eng. 2012;4(2):70–6.

35. Yang Z, Chen J, Proverbs D. Finite element modelling of concrete cover separation failure in FRP plated RC beams. Constr Build Mater. 2003;17(1):3–13.

36. Lubliner J, Oliver J, Oller S, Oñate E. A plastic-damage model for concrete. Int J Solids Struct. 1989;25(3):299–326.